

# X-ray peak profile analysis of $\text{CoAl}_2\text{O}_4$ nanoparticles by Williamson-Hall and size-strain plot methods

H. Irfan<sup>1</sup>, K. Mohamed Racik<sup>2</sup>, S. Anand<sup>2</sup>

<sup>1</sup> Department of Science and Humanities, SAMS engineering college and Technology, Chennai-102, India

<sup>2</sup> Department of Physics, Loyola College, Chennai – 600034, India

Corresponding author: S. Anand (anandnapoleon@gmail.com)

Received 14 August 2017 ♦ Accepted 25 November 2017 ♦ Published 1 May 2018

**Citation:** Irfan H, Mohamed Racik K, Anand S (2018) X-ray peak profile analysis of  $\text{CoAl}_2\text{O}_4$  nanoparticles by Williamson-Hall and size-strain plot methods. *Modern Electronic Materials* 4(1): 31–40. <https://doi.org/10.3897/j.moem.4.1.33272>

## Abstract

$\text{CoAl}_2\text{O}_4$  nanoparticles were prepared by a sol-gel process using citric acid as chelating agent with different calcination temperatures of 600 to 900 °C. The crystalline spinel cubic phase was confirmed by X-ray diffraction results. High-resolution scanning electron microscopy (HRSEM) revealed that nanoparticles of  $\text{CoAl}_2\text{O}_4$  morphology showed spherical forms with a certain degree of agglomeration. The Williamson-Hall (W-H) method and size-strain method to evaluate the size of crystallites and strain in the  $\text{CoAl}_2\text{O}_4$  nanoparticles peak broadening were applied. Physical parameters such as strain and stress values were calculated for all XRD reflection peaks corresponding to the cubic spinel phase of  $\text{CoAl}_2\text{O}_4$  in the range of 20 to 70° from the modified plot shape by W-H plot assuming a uniform deformation model (UDM), uniform stress deformation model (USDM), uniform deformation energy density model (UDEDM) and by the size-strain plot method (SSP). The  $\text{CoAl}_2\text{O}_4$  NPs crystal size calculated on the W-H plots and the SSP method are in good agreement with the HRSEM Scherrer method.

## Keywords

$\text{CoAl}_2\text{O}_4$ , sol-gel synthesis, strain analysis, W-H analysis, SSP method

## 1. Introduction

Spinel oxide type  $\text{AB}_2\text{O}_4$ , where A and B represent two different sites tetrahedral and octahedral and the oxygen ions form a cubic closed structure, are a class of chemically and thermally stable materials that are suitable for a wide-ranging applications such as catalyst and magnetic materials [1-6]. The distribution of cations A and B, these two sites are influenced by the combination and nature of the two cations and is strongly dependent on the preparation and processing conditions [7, 8]. Spin cation distribution has been given a lot of attention because it

allows understanding the correlations between structure and properties such as color, diffusivity, magnetic behavior and optical properties, which are heavily based on better occupation with these two metal sites [9, 10].

In the class of nanomaterials, cobalt aluminate nanocrystalline spinel ( $\text{CoAl}_2\text{O}_4$ ) is known as blue Thenard, commonly used as a catalyst, color filter for automotive lamps and pigment layer on luminescent materials due to their optical properties, thermal chemical, peculiar stability and photochemistry [11, 12]. In recent years, much work has been done in preparation for nanoscale  $\text{CoAl}_2\text{O}_4$  for optical properties. A variety of methods such as com-

bustion [13], Pechni [14], sol-gel [15, 17], microemulsion [16] and plant extract- assisted combustion method [18, 19] have been successfully treated for the preparation of CoAl<sub>2</sub>O<sub>4</sub> nanoparticles.

It is known that the crystallite size and strain are of a pattern that the two main key factors lead to the expansion of XRD diffraction peaks [20, 21]. The crystallite size introduced for the first time by Scherrer in 1918 [20], which is mentioned to the size of a single crystal inside the particles or grains, and it is different from particle size or grain size where the single particle or grain can be comprised into several crystal aggregates. Lattice strain is affected by crystal imperfection such as dislocations and point defects [22]. Other two more types are lattice strains in a crystal, that is, uniform and non-uniform strains. However, only the non-uniform strain will cause the broadening of the Peak [23]. There are some methods for deformation sizing in materials represented by Scherrer [20, 24], Williamson-Hall [25, 26], Strain-size plot and Warren-Averbach methods [27, 28]. Scherrer and Williamson-Hall methods set both maximum half width (FWHM) values and integral breaths, while the Warren-Averbach method refers to the Fourier coefficient profile [29]. From the Warren-Averbach method is a bit of time method and mathematically cumbersome [27, 30].

In this study, CoAl<sub>2</sub>O<sub>4</sub> nanoparticles were prepared by the sol-gel method. X-ray diffraction analysis (XRD) and high resolution scanning electron microscopy (HRSEM) to examine nanoparticles Structural and morphological behavior of CoAl<sub>2</sub>O<sub>4</sub> have been used. X-ray peak profile (XPPA) analysis was determined to calibrate the size of the crystallites and strain of CoAl<sub>2</sub>O<sub>4</sub> nanoparticles based on UDM, USDM and UDEDM models. This work discussed the importance of W-H models and SSP method in calibration of crystalline size and strain parameters for CoAl<sub>2</sub>O<sub>4</sub> nanoparticles.

## 2. Materials and Experimental

CoAl<sub>2</sub>O<sub>4</sub> nanoparticles were synthesized using Co(NO<sub>3</sub>)<sub>2</sub>·6H<sub>2</sub>O (LOBA chemie Ltd), Al(NO<sub>3</sub>)<sub>3</sub>·9H<sub>2</sub>O (Merck), citric acid and deionized water. All of the chemicals above were of analytical grade and were used directly without further purification.

CoAl<sub>2</sub>O<sub>4</sub> were prepared by a sol-gel method using citric acid as a chelating agent. First, a certain amount of cobalt nitrate (Co(NO<sub>3</sub>)<sub>2</sub>·6H<sub>2</sub>O) and aluminum nitrate (Al(NO<sub>3</sub>)<sub>3</sub>·9H<sub>2</sub>O) dissolved in deionized water. After that, appropriate amount of citric acid was added to the solution above with magnetic stirring. The molar ratio of metal ions to citric acid was 1:2. The mixed solution was continuously stirred for 1 hour and then heated to 80 °C until a highly viscous gel was formed. Then the gels were dried in a 110 °C oven and then calcined at desired temperatures (600-900 °C) for 5 h.

X-ray diffraction pattern powder (XRD) was performed on a Bruker D8 Advance X-ray diffractometer.

Morphological analysis and energy dispersion X-ray analysis was performed using EDAX attached to the high resolution scanning electron microscope (HRSEM, FEI, Quanta 200F).

## 3. Results and Discussions

### 3.1. Powder XRD analysis

The crystalline structure of the prepared samples was determined by XRD models reached between 2θ of (20) to (70°). Fig. 1 shows XRD spectra of CoAl<sub>2</sub>O<sub>4</sub> nanoparticles annealed at 600-900 °C for 5 h. Different diffraction peaks are observed in the model and the location of these peaks is very well matched to spinel cubic CoAl<sub>2</sub>O<sub>4</sub> (JCPDS Card No 10-458), indicating the cobalt aluminate phase formation. The intensity of the diffraction peaks increases with the increase in the annealing temperature, which is associated with increased crystallinity. Similar reports were reported by Umapathy et al. [31] and Valan et al [32]. No peaks corresponding to any other material or element are observed, which means that the firing temperature used (900 °C) was sufficient for the preparation of high purity CoAl<sub>2</sub>O<sub>4</sub>. Strong, sharp and narrow diffraction peaks have shown that the synthesized product was well crystallized.

### 3.2. Crystallite size and strain determination

#### 3.2.1. Scherrer method

In general, X-ray diffraction analysis by peak width is due to instrumental amplification, increase in crystallite size and lattice strain due to dislocation [33]. Unbundling these contributions must collect a diffraction pattern of a standard material such as silicon to determine instrumental enlargement [34]. The corrected instrumental broadening β<sub>hkl</sub> [33] corresponding to peak CoAl<sub>2</sub>O<sub>4</sub> diffraction was estimated using the equation,

$$\beta_D^2 = [(\beta_{\text{measured}}^2) - (\beta_{\text{instrumental}}^2)]^{1/2} \quad (1)$$

It is well known that the Scherrer formula provides only the lower limit of crystallite size. The size of crystalline nanoparticles is estimated by the Scherrer formula,

$$D = \frac{K\lambda}{\beta \cos \theta} \quad (2)$$

Where, *D* is the volume weighted crystallite size (nm), *k* is the shape factor (*k* = 0.94), λ is the X-ray wavelength (1.54056 Å), θ is the diffraction angle of Bragg and β is the expanded diffraction peak measured at FWHM (in radians). The size of crystallites of CoAl<sub>2</sub>O<sub>4</sub> nanoparticles are shown in Table 1. Crystallite size is increased with increasing temperature of CoAl<sub>2</sub>O<sub>4</sub> NPs. It is possible on firing effect, because the highly energy-consuming sol-gel method requires rather a more reaction time to form the

ending products. The higher temperature calcination can increase the growth of the crystalline dimension in the nucleation centers, thus limiting the larger dimension [35].

### 3.2.2 Williamson-Hall Method

#### Uniform Deformation Model (UDM)

In many cases, X-ray diffraction patterns are influenced not only by the size of crystallites, but possibly also by lattice strain and lattice defects. Williamson-Hall analysis is a simplified integral breath method, clearly differentiates the armature size and strain induced deformation peak considering the broadening of the peak width as a function of 2 theta. Individual contribution to the line broadening of a Bragg reflection line can be expressed as:

$$\beta_{hkl} = \beta_s + \beta_D \tag{3}$$

Where  $\beta_{hkl}$  represents the full width at half maximum (FWHM) of a radiant peak, and  $\beta_s$   $\beta_D$  are the width due to the size strain, respectively. In the W-H relation it is assumed that the strain is uniform throughout the crystallographic direction, is given by  $\beta_{hkl}$

$$\beta_{hkl} = (k\lambda/D\cos\theta) + 4\epsilon \tan\theta \tag{4}$$

Rearranging Eq. (4) gives

$$\beta_{hkl} \cos\theta = (k\lambda/D) + 4\epsilon \sin\theta \tag{5}$$

Here  $D$  and  $\epsilon$  correspond to the value of the crystallite size and the value of the microstrain respectively. By potting  $4\sin\theta$ , the average size of the crystallites and the strain can be estimated by the Y-intercept extrapolation and the slope of the line; See fig. 2.

#### Uniform Stress Deformation Model (USDM)

According to Hooke’s law, within the elastic limit, there exists a linear proportionality relation between the stress ( $\sigma$ ) and strain ( $\epsilon$ )

$$\sigma = E \epsilon \tag{6}$$

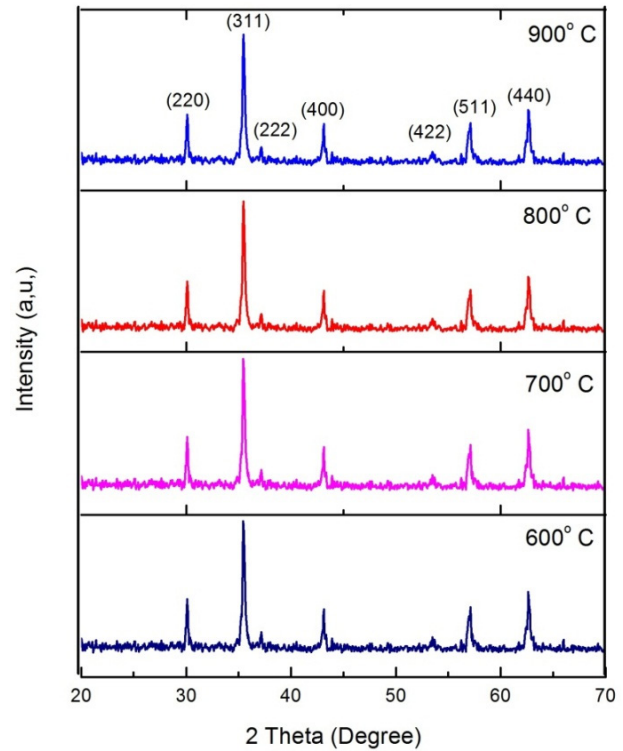


**Figure 1.** XRD pattern of CoAl<sub>2</sub>O<sub>4</sub> nanoparticles annealed at 600–900 °C

where  $E$  is the elasticity modulus or Young’s modulus. This equation is an approximation that is valid for the significantly small strain. Hence, by assuming that the lattice deformation stress is uniform in the second term of equation signifying UDM and is replaced by  $\epsilon = (\sigma/E)$  and the modified Eq. (5) is given by

$$\beta_{hkl} \cos\theta = (K\lambda/D) + (4\sigma \sin\theta/E_{hkl}) \tag{7}$$

Here  $E_{hkl}$  is Young’s modulus in the direction normal to the set of (hkl) planes. The slope of the straight line between  $4\sin\theta/E_{hkl}$  and  $\beta_{hkl} \cos\theta$  gives the uniform stress and the crystallite size  $D$  easily determined from the intercept (Fig. 3). Young’s modulus  $E_{hkl}$  for samples with a cubic crystal phase is related to their elastic compliances  $S_{ij}$  (for CoAl<sub>2</sub>O<sub>4</sub>  $S_{11} = 6.07$ ,  $S_{12} = -3.83$  and  $S_{44} = 7.22$  TPa<sup>-1</sup>) as [35]:

**Table 1.** Geometric parameters of the CoAl<sub>2</sub>O<sub>4</sub> nanoparticles

Sample	Scherrer method		Williamson-Hall method								Size-Strain method		HRSEM	
	$D$ (nm)	$D$ (nm)	$\epsilon$ no unit $\times 10^{-3}$	$D$ (nm)	$\epsilon$ no unit $\times 10^{-3}$	$\sigma$ (MPa)	$D$ (nm)	$\epsilon$ no unit $\times 10^{-3}$	$\sigma$ (MPa)	$U$ (KJm <sup>-3</sup> )	$D$ (nm)	$\epsilon$ no unit $\times 10^{-3}$	$\sigma$ (MPa)	$D$ (nm)
600	19.98	21.07	0.0236	21.07	0.0576	228.3	21.23	0.1152	231.9	108.6	20.11	0.00278	135.3	18.76
700	21.71	23.76	0.0827	24.58	0.1394	259.6	24.70	0.2788	264.3	138.5	21.39	0.00485	165.9	20.93
800	22.50	25.44	0.0010	25.58	0.2419	286.2	25.49	0.0483	216.2	98.6	23.79	0.01916	263.4	22.34
900	23.08	29.91	0.0016	30.04	0.0852	237.6	30.22	0.0172	102.8	56.8	24.79	0.01991	268.3	24.95

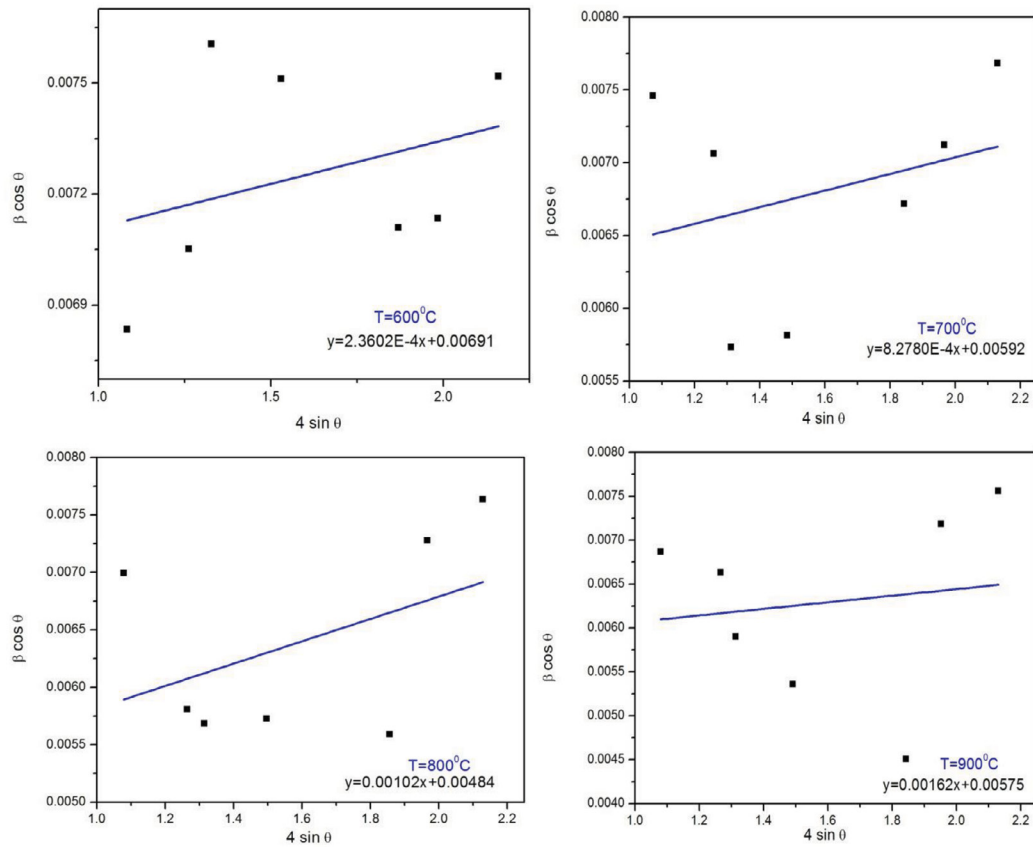


**Figure 2.** UDM plot for  $\text{CoAl}_2\text{O}_4$ -NPs calcined at 600–900 °C.

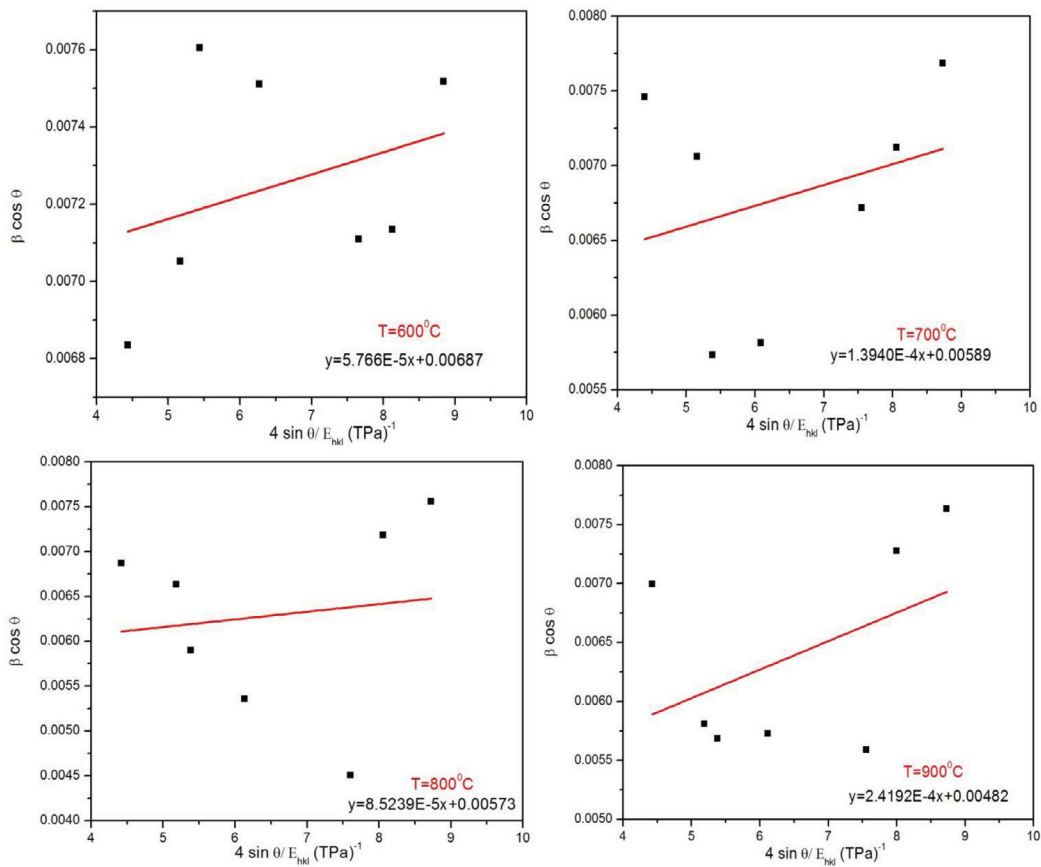


**Figure 3.** USDM plot for  $\text{CoAl}_2\text{O}_4$  – NPs calcined at 600–900 °C.

$$1/E_{hkl} = S_{11} - 2(S_{11} - S_{12} - 0.5S_{44}) (m_1^2 m_2^2 + m_2^2 m_3^2 + m_3^2 m_1^2) \quad (8)$$

where,

$$m_1 = h (h^2 + k^2 + l^2)^{-0.5},$$

$$m_2 = k (h^2 + k^2 + l^2)^{-0.5} \text{ and}$$

$$m_3 = l (h^2 + k^2 + l^2)^{-0.5}.$$

The Young’s modulus  $E_{hkl}$  value for cubic  $\text{CoAl}_2\text{O}_4$  NPs was calculated as 2.44 TPa. Fig. 3 shows the plot of  $\beta_{hkl} \cos\theta$  values as a function of  $4\sin(\theta)/E_{hkl}$ , the uniform deformation stress can be calibrated from the slope.

*Uniform Deformation Energy Density Model (UEDM)*

The following model that can be used to find the energy density of a crystal called Uniform Deformation Energy Density Model (UEDM). Previously, it is assumed that crystals are homogeneous and isotropic. Although in many cases, the assumption of homogeneity and isotropy is not justified. In addition, the proportional constants for strain stress relationship are not widely independent when studying deformation energy density ( $u$ ). For an elastic system that follows Hooke’s law, the energy density (unit energy) can be calculated from the relation  $u=(\epsilon^2 E_{hkl})/2$ . Thus, the equation (9) can be rewritten according to the energy and strain relationship, that is,

$$\beta_{hkl} \cos\theta = (K\lambda/D) + [4\sin\theta(2u/E_{hkl})^{1/2}] \quad (9)$$

Plot of  $\beta_{hkl} \cos\theta$  versus  $4\sin\theta(2u/E_{hkl})^{1/2}$  is shown in Fig. 4. The anisotropic energy density ( $u$ ) is estimated from the slope, and the crystallite size ( $D$ ) of the Y-intercept.

**3.2.3. Size-strain plot method**

The Williamson-Hall plot showed that the line broserning was essentially isotropic. This indicates that the diffraction domains were isotropic and there was also a MicroStrain contribution. However, in the case of isotropic line broadening, it is possible to obtain a better evaluation of the size-strain considering an average “size-strain plot” (SSP), which has relatively less weight gain, is given to high-angle reflections where Accuracy is generally lower. In this approach, the “crystalline dimension” profile is assumed to be described by a Lorentz function and the “strain profile” of a Gaussian function. As a result, we have:

$$(d_{hkl} \beta_{hkl} \cos\theta)^2 = (K/Dv) (d_{hkl}^2 \beta_{hkl} \cos\theta) + (\epsilon/2)^2 \quad (10)$$

where  $K$  is a constant dependent on the shape of the particles; For spherical particles is given as 03/04. In Fig. 5, similar to W-H methods, the term  $(d_{hkl} \beta_{hkl} \cos\theta)^2$  is

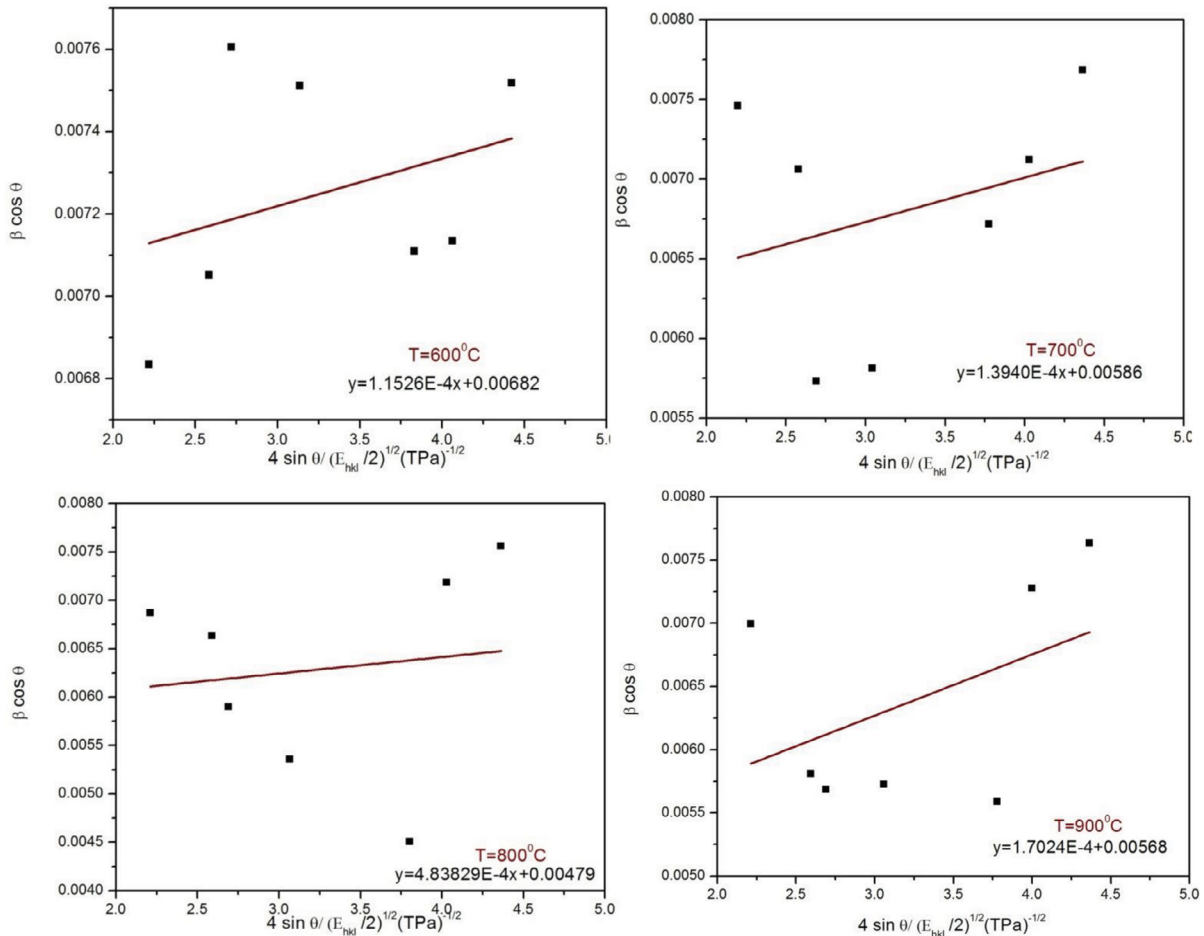


**Figure 4.** UEDM plot for  $\text{CoAl}_2\text{O}_4$ -NPs calcined at 600–900 °C.

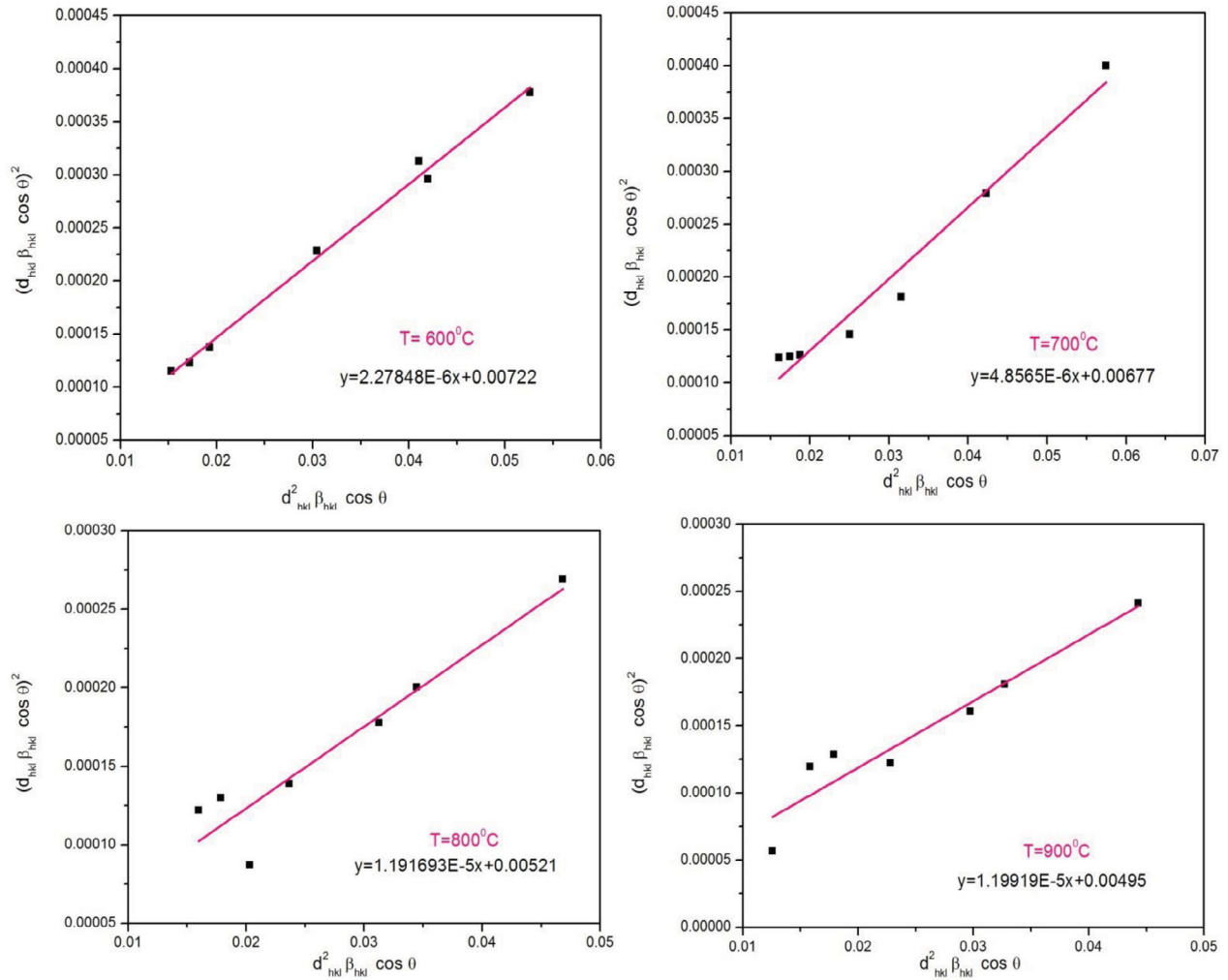


**Figure 5.** Size-strain plot of  $\text{CoAl}_2\text{O}_4$ -NPs calcined at 600–900 °C

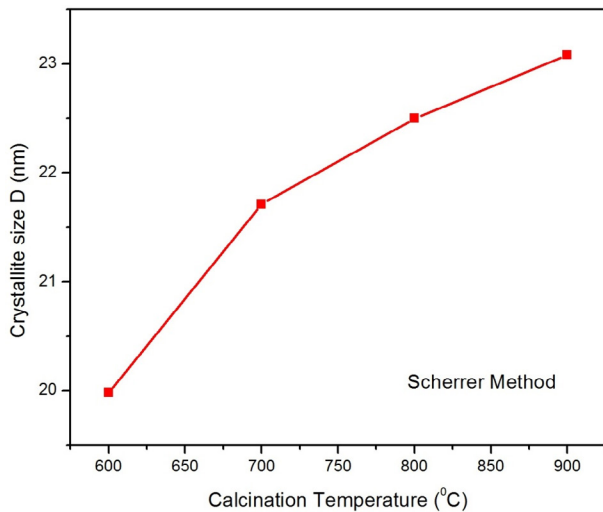


**Figure 6.** Variation of crystallite size ( $D$ ) with calcination temperature obtained from Scherrer method.

plotted with respect to  $d_{hkl}^2 \beta_{hkl} \cos \theta$  for all  $\text{CoAl}_2\text{O}_4$  NPs orientation peaks. In this case, the particle size is determined by the slope of the linearly fitted data and

the intercepted root yields strain. By varying the size of crystallites ( $D$ ) with the result of the calcination temperature obtained by the Scherrer formula, W-H (UDM, USDM and UDEDM) models and SSP methods shown in Figs. 6-8. The values of average crystallite size of different calcined temperature of  $\text{CoAl}_2\text{O}_4$ -NPs obtained from different models are more or less similar, implying that the inclusion of strain in various shapes has a slight variation in the average size of crystallites. By inspecting all the graphs, it is clear that the result of the SSP method is more accurate than UDM, USDM and UDEDM since data is more accurately set in this method, with all high intensity points touching linear adaptation. The geometric parameters of  $\text{CoAl}_2\text{O}_4$  nanoparticles shown in Table 1.

### 3.3. Morphological Studies

The morphology of cobalt aluminate synthesized nanoparticles was studied by high-resolution scanning electron microscopy (HRSEM). From Fig. 9, it can be clearly demonstrated that the obtained nanoparticles are of spherical shape with some groups present in aggregation of

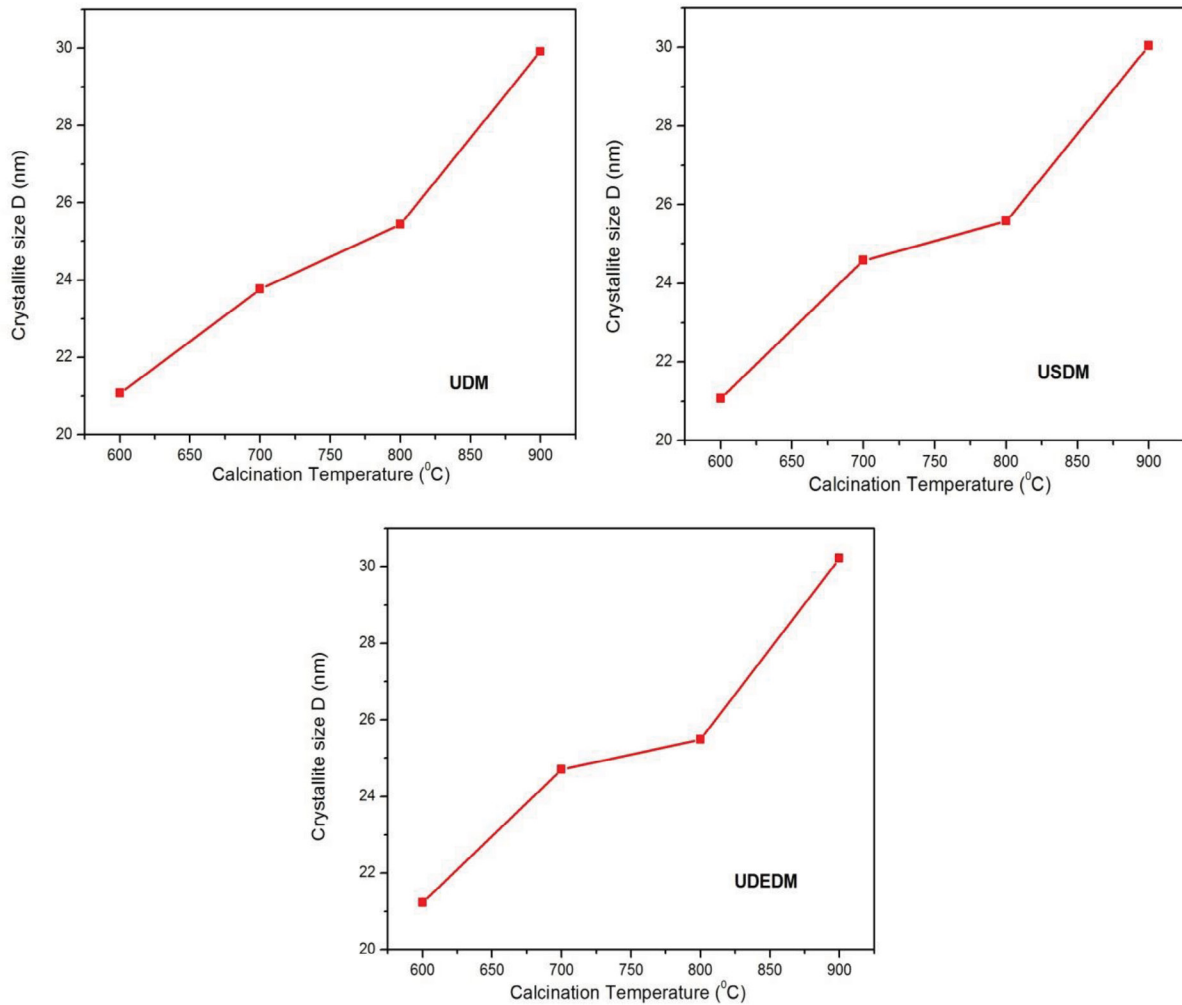


**Figure 7.** Variation of crystallite size ( $D$ ) with calcination temperature obtained from W-H method

spheres. It can be seen from SEM micrographs using ImageJ processing program confirmed the particle size ranges from 18.76 to 24.95 nm. Alida Mazzoli and Orlando Favoni evaluated the particle sizes and size distribution with the use of Scanning Electron Microscopy (SEM) and ImageJ processing program [36].

### 4. Conclusion

$\text{CoAl}_2\text{O}_4$  nanoparticles have been prepared by the sol gel method and are characterized by powder XRD and HRSEM analysis. From the XRD powder analysis, the peak line broadening of  $\text{CoAl}_2\text{O}_4$  nanoparticles due to finite crystallite size and strain were analyzed by Scherrer’s formula, Williamson-Hall method based on UDM, USDM and UEDM models and Size strain plot method. W-H plot has been worked out and established to determine the crystallite size and strain-induced broadening due to lattice deformation. The W-H analysis based on the UDM, USDM and UEDM models are very helpful in calculating the estimation of crystallite size and strain. W-H has been developed and established to determine

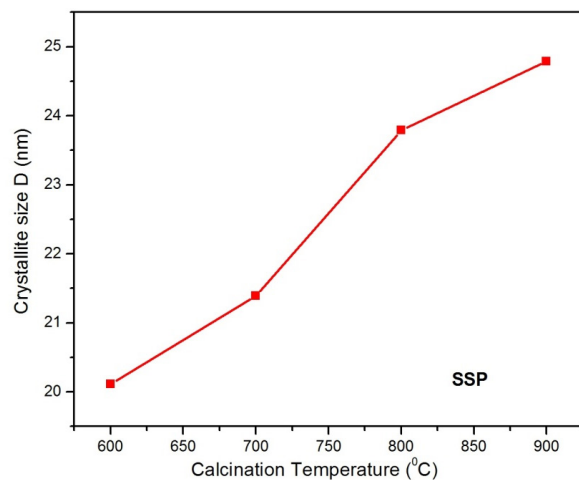


**Figure 8.** Variation of crystallite size ( $D$ ) with calcination temperature obtained from SSP method

the size of crystallites and the elongated induced deformation due to deformation of the network. UDM-based U-DMS, USDM and UEDM analyzes are useful for

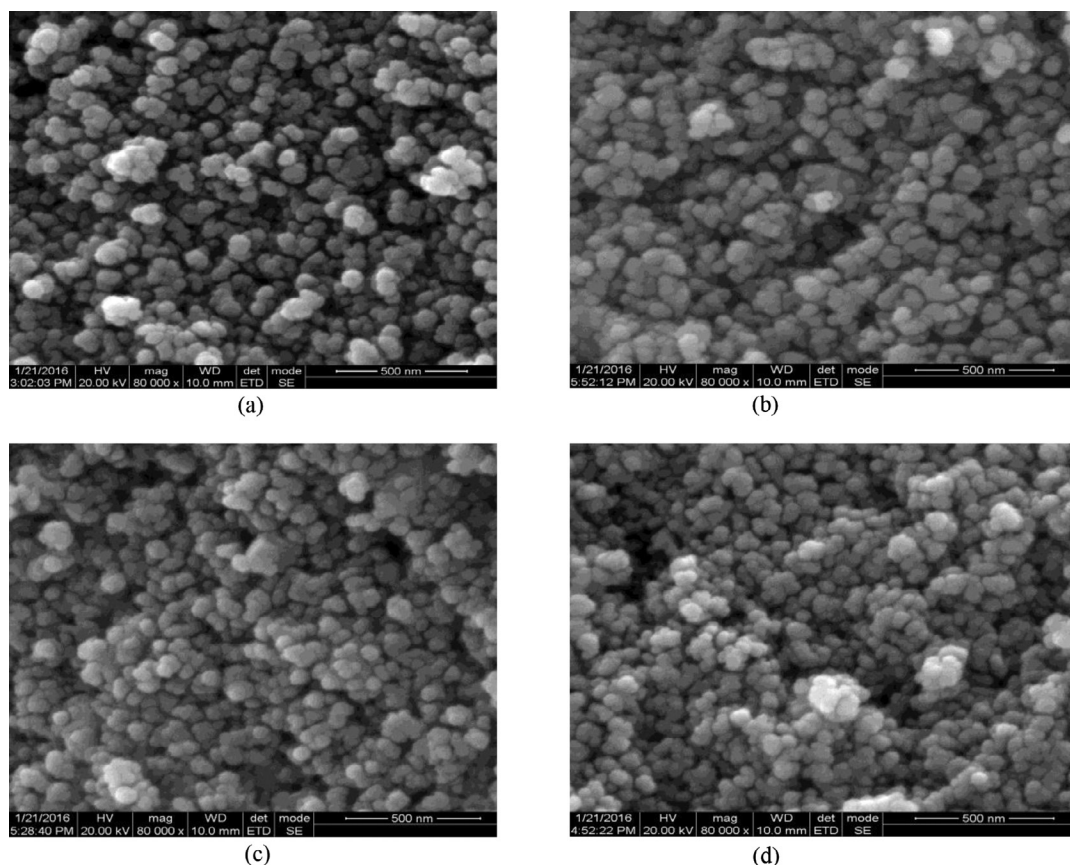


**Figure 9.** HRSEM images of  $\text{CoAl}_2\text{O}_4$  nanoparticles annealed at 600 °C (a), 700 °C (b), 800 °C (c) and 900 °C (d).

calculating dimension estimation and deformation of crystallites. The size of crystallites and strain evaluated by the XRD powder measurements are in good agreement with HRSEM results. The elastic properties of the Young  $S_{ij}$  ( $E_{hkl}$ ) module were estimated by the values of the plane of the lattice (h, k, l). The methods discussed above were very useful in determining the average size of deformation crystals, stress and energy density value,

including the size-strain method; it is highly preferable to set crystal perfection.

## Acknowledgement

The Authors are thankful to Dept. of Nuclear Physics, University of Madras, Chennai for XRD facility.

## References

1. I.H. Gul, A. Maqsood, M. Naeem, M. Naeem Ashiq, Optical, magnetic and electrical investigation of cobalt ferrite nanoparticles synthesized by co-precipitation route, *J. Alloys Compd.* 507 (2010) 201. <https://doi.org/10.1016/j.jallcom.2010.07.155>
2. F. Tielens, M. Calatayud, R. Franco, J.M. Recio, M. Perez-Ramirez, C. Minot, Periodic DFT Study of the Structural and Electronic Properties of Bulk  $\text{CoAl}_2\text{O}_4$  Spinel, *J.Phys. Chem. B* 110 (2006) 988. <https://doi.org/10.1021/jp053375l>
3. A. Manikandan, M. Durka, S. Arul Antony, One-Pot Flash Combustion Synthesis, Structural, Morphological and Opto-Magnetic Properties of Spinel  $\text{Mn}_x\text{Co}_{1-x}\text{Al}_2\text{O}_4$  ( $x = 0, 0.3, \text{ and } 0.5$ ) Nanocatalysts, *S. J Supercond Nov Magn* (2015) 28: 209. <https://doi.org/10.1007/s10948-014-2841-4>
4. S. Suguna, S. Shankar, Saravana Kumar Jaganathan, A. Manikandan, Novel Synthesis of Spinel  $\text{Mn}_x\text{Co}_{1-x}\text{Al}_2\text{O}_4$  ( $x = 0.0 \text{ to } 1.0$ ) Nanocatalysts: Effect of  $\text{Mn}^{2+}$  Doping on Structural, Morphological, and Opto-Magnetic Properties *J. Supercond Nov Magn* (2017) 30: 691. <https://doi.org/10.1007/s10948-016-3866-7>
5. S. Jayasree, A. Manikandan, A.M. Mohideen, C. Uduman, C. Barathiraja, S. Arul Antony, Comparative Study of Combustion Methods, Opto-Magnetic and Catalytic Properties of Spinel  $\text{CoAl}_2\text{O}_4$  Nano- and Microstructures, *Advanced Science, Engineering and Medicine*, 7(8), (2015), pp. 672-682. <https://doi.org/10.1166/aseem.2015.1750>
6. C. Maurizio, N. El Habra, G. Rossetto, M. Merlini, E. Cattaruzza, L. Pandolfo, M. Casarin, XAS and GIXRD Study of Co Sites in

- CoAl<sub>2</sub>O<sub>4</sub> Layers Grown by MOCVD, *Chem. Mater.* 22 (2010) 1933. <https://doi.org/10.1021/cm9018106>
7. V. Mary Teresita, A. Manikandan, B. Avila Josephine, S. Sujatha, S. Arul Anton, Electromagnetic Properties and Humidity-Sensing Studies of Magnetically Recoverable LaMg<sub>x</sub>Fe<sub>1-x</sub>O<sub>3-δ</sub> Perovskites Nano-photocatalysts by Sol-Gel Route, *J Supercond Nov Magn* (2016) 29: 1691. <https://doi.org/10.1007/s10948-016-3465-7>
  8. D.K. Manimegalai, A. Manikandan, S. Moortheswaran, S. Arul Antony, Magneto-Optical and Photocatalytic Properties of Magnetically Recyclable Mn<sub>x</sub>Zn<sub>1-x</sub>S(x = 0.0, 0.3, and 0.5) Nanocatalysts, et al. *J Supercond Nov Magn* (2015) 28: 2755. <https://doi.org/10.1007/s10948-015-3089-3>
  9. A. Walsh, Y. Yan, M.M. Al-Jassim, S.-H. Wei, Electronic, Energetic, and Chemical Effects of Intrinsic Defects and Fe-Doping of CoAl<sub>2</sub>O<sub>4</sub>: A DFT+*U* Study, *J. Phys. Chem. C* 112 (2008) 12044, <https://doi.org/10.1021/jp711566k>
  10. D. Rangappa, T. Naka, A. Kondo, M. Ishii, T. Kobayashi, T. Adschiri, *J. Am. Chem. Soc.* 129 129 (36) (2007) pp 11061–11066. <https://doi.org/10.1021/ja0711009>
  11. P.M.T. Cavalcante, M. Dondi, G. Guarini, M. Raimondo, G. Baldil, Colour performance of ceramic nano-pigments, *Dyes Pigments* 80 (2009) 226. <https://doi.org/10.1016/j.dyepig.2008.07.004>
  12. W.S. Cho, M. Kakihana, Crystallization of ceramic pigment CoAl<sub>2</sub>O<sub>4</sub> nanocrystals from Co–Al metal organic precursor, *J. Alloys Compd.* 287 (1999) 87. [https://doi.org/10.1016/S0925-388\(99\)00059-6](https://doi.org/10.1016/S0925-388(99)00059-6)
  13. T. Mimani, Instant synthesis of nanoscale spinel aluminates, *J. Alloys Compd.* 315 (2001) 123. [https://doi.org/10.1016/S0925-8388\(00\)01262-7](https://doi.org/10.1016/S0925-8388(00)01262-7)
  14. L. Gama, M.A. Ribeiro, B.S. Barros, R.H.A. Kiminami, I.T. Weber, A.C.F.M. Costa, Synthesis and characterization of the NiAl<sub>2</sub>O<sub>4</sub>, CoAl<sub>2</sub>O<sub>4</sub> and ZnAl<sub>2</sub>O<sub>4</sub> spinels by the polymeric precursors method, *J. Alloys Compd.* 483 (2009) 453. <https://doi.org/10.1016/j.jallcom.2008.08.111>
  15. F.L. Yu, J.F. Yang, J.Y. Ma, J. Du, Y.Q. Zhou, Preparation of nano-sized CoAl<sub>2</sub>O<sub>4</sub> powders by sol–gel and sol–gel-hydrothermal methods, *J. Alloys Compd.* 468 (2009) 443, <https://doi.org/10.1016/j.jallcom.2008.01.018>
  16. J. Chandradass, M. Balasubramanian, K.H. Kim, Size effect on the magnetic property of CoAl<sub>2</sub>O<sub>4</sub> nanopowders prepared by reverse micelle processing, *J. Alloys Compd.* 506 (2010) 395. <https://doi.org/10.1016/j.jallcom.2010.07.014>
  17. M. Zayat, D. Levy, Blue CoAl<sub>2</sub>O<sub>4</sub> Particles Prepared by the Sol–Gel and Citrate–Gel Methods, *Chem. Mater.* 12 (2000) 2763. <https://doi.org/10.1021/cm001061z>
  18. A. Manikandan, M. Durka, M. Amutha Selvi, S. Arul Antony, Sesamum indicum Plant Extracted Microwave Combustion Synthesis and Opto-Magnetic Properties of Spinel Mn<sub>x</sub>Co<sub>1-x</sub>Al<sub>2</sub>O<sub>4</sub> Nano-Catalysts, *Journal of Nanoscience and Nanotechnology*, 16(1), (2016) pp. 448-456. <https://doi.org/10.1166/jnn.2016.10632>
  19. A. Manikandan, M. Durka, M. Amutha Selvi, and S. Arul Antony, Aloe vera Plant Extracted Green Synthesis, Structural and Opto-Magnetic Characterizations, *Journal of Nanoscience and Nanotechnology*, 16 (2016) 357–373. <https://doi.org/10.1166/jnn.2016.10621>
  20. A.R Stokes, A.J.C. Wilson, The diffraction of X rays by distorted crystal aggregates – I, *Proceedings of Physica* 56 (1944) 174. <https://doi.org/10.1088/0959-5309/56/3/303>
  21. K. Ramakanth, Basic of diffraction and its application, I K International Publishing House, 2007.
  22. A. Jose, M.F.G. Rodriguez, Synthesis, Properties, and Applications of Oxide Nanomaterials, first ed., Wiley-Interscience, 2007.
  23. Allen W. Burton, Kenneth Ong, Thomas Rea, Ignatius Y. Chan, On the estimation of average crystallite size of zeolites from the Scherrer equation: A critical evaluation of its application to zeolites with one-dimensional pore systems, *Microporous and Mesoporous Materials* 117 (2009) 75–90. <https://doi.org/10.1016/j.micromeso.2008.06.010>
  24. G.K. Williamson, W.H. Hall, X-ray line broadening from filed aluminium and wolfram, *Acta Metallurgica* 1(1953) 22–31. [https://doi.org/10.1016/0001-6160\(53\)90006-6](https://doi.org/10.1016/0001-6160(53)90006-6)
  25. K. Venkateswarlu, A. Chandra Bose, N. Rameshbabu, X-ray peak broadening studies of nanocrystalline hydroxyapatite by Williamson–Hall analysis, *Physica B: Condensed Matter* 405 (2010) 4256–4261. <https://doi.org/10.1016/j.physb.2010.07.020>
  26. B.E.A. Warren, B.L. Averbach, The Effect of Cold-Work Distortion on X-Ray Patterns, *Journal of Applied Physics* 21 (1950) 595–599. <https://doi.org/10.1063/1.1699713>
  27. J. Gubicza, G. Ribarik, I. Bakonyi, T. Ungar, Crystallite-Size Distribution and Dislocation Structure in Nanocrystalline Hf Ni<sub>3</sub> Determined by X-Ray Diffraction Profile Analysis, *Journal of Nanoscience and Nanotechnology* 1 (2001) 343–348. <https://doi.org/10.1166/jnn.2001.039>
  28. S. Vives, E. Gaffet, C. Meunier, X-ray diffraction line profile analysis of iron ball milled powders, *Materials Science and Engineering A366* (2004) 229–238. [https://doi.org/10.1016/S0921-5093\(03\)00572-0](https://doi.org/10.1016/S0921-5093(03)00572-0)
  29. A.B. Djurasic, Y.H. Leung, K.H. Tam, L. Ding, W.K. Ge, H.Y. Chen, S. Gwo, Green, yellow, and orange defect emission from ZnO nanostructures: Influence of excitation wavelength *Appl. Phys. Lett.* 88 (2006) 103107. <https://doi.org/10.1063/1.2182096>
  30. G. Srinet, R. Kumar, V. Sajal, High T<sub>c</sub> ferroelectricity in Ba-doped ZnO nanoparticles, *Mater. Lett.* 126(2014)274–277. <https://doi.org/10.1016/j.matlet.2014.04.054>
  31. V. Umapathy, A. Manikandan, P. Ramu, S. Arul Antony, P. Neeraja, Synthesis and Characterization of Fe<sub>3</sub>(MoO<sub>4</sub>)<sub>3</sub> Nano-Photocatalyst by Simple Sol–Gel Method, *Journal of Nanoscience and Nanotechnology*, 16(1), (2016), pp. 987-993. <https://doi.org/10.1166/jnn.2016.10616>
  32. M. F. Valan, A. Manikandan, S. Arul Antony, Novel Synthesis and Characterization Studies of Magnetic Co<sub>3</sub>O<sub>4</sub> Nanoparticles, *Journal of Nanoscience and Nanotechnology*, 15(6), (2015), pp. 4580-4586. <https://doi.org/10.1166/jnn.2015.9776>
  33. K. Chinnaraj, A. Manikandan, P. Ramu, S. Arul Antony, P. Neeraja, Comparative Studies of Microwave- and Sol-Gel Assisted Combustion Methods of Fe<sub>3</sub>O<sub>4</sub> Nanostructures: Structural, Morphological, Optical, Magnetic, and Catalytic Properties., *J Supercond Nov Magn* 28 (2015) 179-190. <https://doi.org/10.1007/s10948-014-2835-2>
  34. S. Harjo, Y. Tomota, S. Torii, T. Kamiyama, Residual Thermal Phase Stresses in α-γ Fe-Cr-Ni Alloys Measured by a Neutron Diffraction Time-of-Flight Method, *Materials Transactions*, 43 (2002) 1696-1702. <https://doi.org/10.2320/matertrans.43.1696>
  35. M.A. Tagliente, M. Massaro, Strain-driven (0 0 2) preferred orientation of ZnO nanoparticles in ion-implanted silica, *Nucl. Instrum*

- Methods Phys. Res. B. 266 (2008) 1055. <https://doi.org/10.1016/j.nimb.2008.02.036>
36. Alida Mazzoli, Orlando Favoni, Particle size, size distribution and morphological evaluation of airborne dust particles of diverse woods by Scanning Electron Microscopy and image processing program, Powder Technology 225 (2012) 65–71. <https://doi.org/10.1016/j.powtec.2012.03.033>